manuscript ra5102 for review

Acta Cryst B
STRUCTURAL SCIENCE
CRYSTAL ENGINEERING
MATERIALS

Low temperature investigation of iron-rich oxoborates vonsenite and hulsite: thermal deformations of crystal structure and cascades of magnetic transitions

Yaroslav P. Biryukov, Almaz L. Zinnatullin, Mikhail A. Cherosov, Andrey P. Shablinskii, Roman V. Yusupov, Rimma S. Bubnova, Farit G. Vagizov, Stanislav K. Filatov and Igor V. Pekov

Category: *research papers*

Co-editor:

Professor R. Cerny

Laboratoire de Cristallographie, University of Geneva, 24 quai Ernest-Ansermet, CH-1211 Geneva 4, Switzerland

Telephone: 41(22)379 6450

Fax: 41(22)379 6108

Email: Radovan.Cerny@unige.ch

Submitting author:

Yaroslav P. Biryukov

Institute of Silicate Chemistry of the Russian Academy of Sciences (ISC RAS), Makarova emb., 2, Saint Petersburg, 199034, Russian Federation

Telephone: +78123288596

Fax: +78123288596

Email: y.p.biryukov@gmail.com

Low temperature investigation of iron-rich oxoborates vonsenite and hulsite: thermal deformations of crystal structure and cascades of magnetic transitions

Authors

Yaroslav P. Biryukov[a], Almaz L. Zinnatullin[b], Mikhail A. Cherosov[b], Andrey P. Shablinskii[a], Roman V. Yusupov[b], Rimma S. Bubnova[a]*, Farit G. Vagizov[b], Stanislav K. Filatov[c] and Igor V. Pekov[d]

[a] Institute of Silicate Chemistry of the Russian Academy of Sciences (ISC RAS), Makarova emb., 2, Saint Petersburg, 199034, Russian Federation

[b] Kazan Federal University, Kremlyovskaya Str., 18, Kazan, 420008, Russian Federation

[c]Institute of Earth Sciences, Department of Crystallography, Saint Petersburg State University, Universitetskaya Emb., 7/9, Saint Petersburg, 199034, Russian Federation

[d]Faculty of Geology, Moscow State University, Leninskie Gory, 1, Moscow, 119991, Russian Federation

Correspondence email: rimma_bubnova@mail.ru

Funding information Processing of experiments, interpretation of data and their generalization were funded by the Ministry of Science and Higher Education of the Russian Federation (contract No. 0097-2019-0013 to Institute of Silicate Chemistry of the Russian Academy of Sciences (ISC RAS), Yaroslav P. Biryukov, Rimma S. Bubnova, Andrey P. Shablinskii); magnetometry studies were funded by the Ministry of Science and Higher Education of the Russian Federation (contract No. 0671-2020-0050 to Kazan Federal University, Mikhail A. Cherosov, Roman V. Yusupov); LTXRD experiments were funded by the Russian Foundation for Basic Research (grant No. 18-29-12106 to Rimma S. Bubnova, Andrey P. Shablinskii, Stanislav K. Filatov).

Synopsis Vonsenite and hulsite were investigated by a set of *in situ* low temperature methods. Cascades of magnetic transitions were revealed in both oxoborates and its critical temperatures were determined. Anomalies in cell parameters and thermal expansion of the oxoborates at critical temperatures were observed.

Abstract This work is devoted to investigation of magnetic properties and thermal behavior of natural oxoborates vonsenite and hulsite in the temperature range 5–500 K. Local environment, oxidation states of Fe and Sn atoms as well as charge distribution are determined using Mössbauer spectroscopy and are in accordance with a refinement of a crystal structure of hulsite and its atomic displacement parameters from single-crystal X-ray diffraction data (SCXRD) in anisotropic approximation for the first time. Magnetic properties were determined by vibrating sample magnetometry (VSM) ($5 \leq T \leq 400$ K) and reported for the first time for iron-rich hulsite. Both oxoborates show very complex magnetic behavior. Cascades of magnetic transitions are revealed and its critical temperatures are determined. Sequences of magnetic transitions in vonsenite and hulsite with an increase in temperature were found to be as follows "magnetically ordered state → partial magnetic ordering → paramagnetic state" and "magnetically ordered state, weak ferromagnet/antiferromagnet → magnetically ordered state, ferrimagnet-like → magnetically ordered state, weak ferromagnet → partial magnetic ordering, antiferromagnet → paramagnetic state" respectively. According to low temperature X-ray diffraction (LTXRD) data ($93 \leq T \leq 500$ K), these processes are accompanied by anomalies in cell parameters and thermal expansion of the oxoborates at critical temperatures. A strong negative volume thermal expansion is observed for both oxoborates at temperatures below ~120 K, which is accompanied with a compression of its crystal structures.

Keywords: Vonsenite; Hulsite; Ludwigite group; Pinakiolite group; Crystal structure

1. Introduction

Iron-rich oxoborates dimorphous in part of the end-member $Fe^{2+}{}_2Fe^{3+}(BO_3)O_2$, orthorhombic vonsenite (Takéuchi, 1956; Swinnea & Steinfink 1983) and monoclinic hulsite (Yamnova *et al.,* 1975; Konnert *et al*., 1976; Yamnova *et al.,* 1978), belong to ludwigite (*Pbam*) and pinakiolite (*P*2/*m*) groups, respectively. Both minerals are typical for magnesian skarns and related boron deposits (Aleksandrov & Troneva, 2008). Its crystal structures contain the isolated $[BO_3]^{3-}$ triangles and metal-oxygen $[MO_6]^{n-}$ octahedra (*M* positions are occupied by Fe(II,III) with minor Mg^{2+}, Mn^{2+}, Al^{3+} and Sn^{4+} admixtures) (Takéuchi 1956; Konnert *et al*., 1976; Yamnova *et al.,* 1975; Yamnova *et al*., 1978; Swinnea & Steinfink 1983; Biryukov *et al*., 2020). There are four and five *M* positions for cations in the crystal structure of vonsenite and hulsite, respectively. In terms of oxocentred polyhedra, the structures are described as frameworks composed of the $[OM_4]^{n+}$ tetrahedra and $[OM_5]^{n+}$ pyramids (Biryukov *et al*., 2020).

Nowadays vonsenite- and hulsite-like compounds are considered as promising ones for a design of magnetic materials with attractive properties such as cascades of magnetic transitions, a coexistence of paramagnetism and magnetic ordering, charge ordering, spin-glass behavior and geometric frustrations

(Mir *et al*., 2001; Continentino *et al*., 2005; Freitas *et al*., 2008; Medrano *et al*., 2018; Knyazev *et al*., 2019; Galdino *et al*., 2019; Medrano *et al*., 2021).

Synthetic vonsenite $Fe^{2+}{}_2Fe^{3+}(BO_3)O_2$ is the most studied object of $M^{2+}{}_2M^{3+}(BO_3)O_2$ family (Attfield *et al*., 1992; Guimarães *et al*., 1999; Mir *et al*., 2001; Douvalis *et al*., 2002; Whangbo *et al*., 2002; Larrea *et al*., 2004; Freitas *et al*., 2008; Bordet & Suard, 2009; Maignan *et al*., 2017; Martin *et al*., 2017; Knyazev *et al*., 2019; Damay *et al*., 2020). According to (Guimarães *et al*., 1999; Bordet & Suard, 2009), there are two types of one-dimensional (1D) magnetic subsystems, the Fe(3)–Fe(1)–Fe(3) and Fe(4)–Fe(2)–Fe(4) triads forming three-leg ladders (3LL) running along the *c* axis. A cascade of magnetic transitions was obtained with a decrease in temperature: an antiferromagnetic at T_N = 112 K and a weak ferromagnetism below T_C = 70 K. Between 112 and 70 K, antiferromagnetism and paramagnetism coexist. Below 40 K, the compound becomes antiferromagnetic again. Each subsystem orders magnetically at different temperatures. The antiferromagnetic transition takes place in the Fe(4)–Fe(2)–Fe(4) triads, the weak ferromagnetism at T_C arises from the Fe(3)–Fe(1)–Fe(3) subsystem.

On the other hand, there is a lack of works devoted to investigation of properties of natural or synthetic hulsite-like compounds. Moreover, there are only three synthetic hulsite-like compounds known to date: $Ni_{5.33}Sb_{0.67}B_2O_{10}$, $Co_{5.52}Sb_{0.48}(BO_3)O_2$ and $Ni_{5.15}Sn_{0.85}(BO_3)O_2$ (Bluhm *et al*., 1990; Freitas *et al*., 2010; Medrano *et al*., 2018) and none of them are iron-containing. It was shown in (Freitas *et al*., 2010) that there are two types of two-dimensional (2D) magnetic subsystems formed by parallel sheets, that held together by corner-linking to the boron-oxygen triangles and to the oxygen octahedra around the *M*(5) metal sites (Freitas *et al*., 2010). These synthetic compounds exhibit magnetic transitions with a decrease in temperature. Thus, we find it is important to investigate crystallochemical, thermal and magnetic properties of iron-rich hulsite.

Recently we investigated crystal and magnetic structures, thermodynamic and magnetic properties of iron-containing borates such as synthetic norbergite-like $Fe_3(BO_4)O_2$ and calcite-like $FeBO_3$, natural vonsenite and hulsite (Biryukov *et al*., 2018; 2019; 2020) by *in situ* high-temperature Mössbauer spectroscopy and X-ray diffraction. Such a set of highly precise methods works excellent in order of investigation of a number of processes occurred with an increase or a decrease in temperature: a cation distribution, the Fe^{2+} to Fe^{3+} oxidation, magnetic transitions and its influence on thermal behavior of the borates.

Here we report for the first time the data on thermal behavior of the iron-rich oxoborates vonsenite and hulsite investigated by the set of *in situ* low temperature methods: single-crystal and powder X-ray diffraction, Mössbauer spectroscopy and magnetometry. A special attention is paid to a description of mechanisms of thermal deformations of the crystal structures of both oxoborates.

2. Experimental

2.1. Materials

The minerals were collected from the Titovskoe boron skarn deposit, Sakha Republic, Russia. Crystals of hulsite suitable for single-crystal X-ray diffraction experiments were selected using a LOMO (Russia) binocular microscope and then checked on a Bruker SMART APEX II diffractometer. Elemental compositions of the samples were determined in (Biryukov *et al*., 2020). Empirical formulas of vonsenite and hulsite calculated on the basis on 5 oxygen atoms per formula unit (*apfu*) are $(Fe^{2+}_{1.86}Mg_{0.13})_{\Sigma 1.99}(Fe^{3+}_{0.92}Mn^{2+}_{0.05}Sn^{4+}_{0.02}Al_{0.02})_{\Sigma 1.01}(BO_3)O_2$ and $(Fe^{2+}_{1.90}Mg_{0.11})_{\Sigma 2.01}(Fe^{3+}_{0.88}Mn^{2+}_{0.06}Sn^{4+}_{0.05}Al_{0.01})_{\Sigma 1.00}(BO_3)O_2$, respectively. These data are in accordance with the Mössbauer spectroscopy one. An information on mean analytical results of vonsenite and hulsite is given in Table 1S in (Biryukov *et al*., 2020).

2.2. Single-crystal X-ray diffraction

Single-crystal X-ray diffraction data were collected using a Bruker SMART APEX II diffractometer equipped with a CCD detector using Mo *Kα* radiation. More than one hemisphere of three-dimensional data was collected by the CCD detector and frame widths of 0.5 in ω, with 60 s used to acquire each frame. The data were corrected for Lorentz, polarization and background effects using Bruker programs APEX. A semi-empirical absorption-correction based on the intensities of equivalent reflections was applied in the SADABS program (Krause *et al*., 2015). The crystal structure of hulsite were solved by charge flipping and refined using JANA2006 program suite (Petříček *et al*., 2014). Experimental details are given in Table 1. Atomic coordinates, displacement parameters and selected bond distances are given in Tables S1–S3.

Crystal structure of vonsenite at 293 and 400 K was refined previously and supporting information can be found in (Biryukov *et al*., 2020; CCDC 2004063).

Table 1

Crystallographic and experimental data of hulsite collected at 293 K.

Mineral name	Hulsite
Chemical formula	$Fe_{2.80}Mg_{0.18}Sn_{0.02}(BO_3)O_2$
M_r	253.4
Crystal system, space group	Monoclinic, *P*2/*m*
Temperature (K)	293
a, *b*, *c* (Å)	10.638 (3), 3.063 (2), 5.445 (5)
β (°)	93.38 (4)
V (Å^3)	177.1 (2)
Z	2
Radiation type	Mo $K\alpha$
μ (mm^{-1})	11.36
Crystal size (mm)	0.06 × 0.03 × 0.01
Data collection	
Diffractometer	Bruker Smart APEX II
Absorption correction	Multi-scan
No. of measured, independent and observed [$I > 3\sigma(I)$] reflections	1449, 346, 218
R_{int}	0.081
$(\sin \theta/\lambda)_{max}$ (Å^{-1})	0.686
Refinement	
$R[F^2 > 2\sigma(F^2)]$, $wR(F^2)$, S	0.063, 0.065, 1.74
No. of reflections	345
No. of parameters	51
No. of restraints	3
$\Delta\rho_{max}$, $\Delta\rho_{min}$ (e Å^{-3})	1.28−1.14

The crystal structures were visualized using VESTA (Momma & Izumi, 2011).

2.3. Mössbauer spectroscopy

Mössbauer experiments were performed in transmission geometry using a conventional spectrometer (WissEl, Germany) operating in constant acceleration mode. Measurements were carried out within the temperature range 5–400 K using helium continuous flow cryostat (model CFICEV from ICE Oxford, UK) and Mössbauer furnace MBF-1100 equipped with TR-55 temperature controller (WissEl). Temperature accuracy of ±0.1 K was controlled by CryoCon 32B controller during low-temperature experiments. The ^{57}Co(Rh) with an activity of about 40 mCi and the ^{119m}Sn($CaSnO_3$) with an activity of about 15 mCi (both RITVERC GmbH, Russia) were used as sources for resonance radiation. The spectrometer velocity scale was calibrated using thin metallic iron foil at room temperature. The spectra were least-squares fitted with the assumption that the shape of lines is

Lorentzian using SpectrRelax software (Matsnev & Rusakov, 2012). Values of isomer shifts are reported versus centers of gravity of α-Fe and SnO_2 at room temperature.

2.4. Magnetic properties

Measurements of bulk magnetic properties were performed by vibrating sample magnetometry (VSM) technique on Quantum Design PPMS-9. Magnetic studies were carried out in the temperature range 5–400 K and external magnetic fields up to 9 T.

2.5. X-ray powder diffraction

Powder diffraction data at room temperature were collected using a Rigaku MiniFlex II diffractometer (Co *Kα,* 2Θ = 5–90º, step 0.02º). The phase composition was determined using PDXL integrated X-ray powder diffraction software (Sasaki *et al*., 2010) and PDF-2 2016 from the ICDD. X-ray phase analysis revealed that the polycrystalline samples of vonsenite and hulsite contained in its compositions magnetite Fe_3O_4 and diopside $CaMg(Si_2O_6)$ as impurities in a quantity of about 0.6 wt% and 2–6 wt%, respectively.

Low temperature X-ray powder diffraction experiments were conducted using a Rigaku Ultima IV diffractometer with a thermal attachment R-300 (Co *K*α radiation, 40 kV and 35 mA, reflection geometry, D/teX Ultra high-speed detector, forvacuum, nitrogen cooling, 2Θ = 10–75°, temperature range: 93–313 K for vonsenite and 93–500 K for hulsite, step width: 2–5 K, heating rate: 0.6 K/min). Experimental data processing by the Rietveld refinement, approximation of temperature dependencies of unit cell parameters and drawing figures of thermal expansion coefficients (α) were performed using RietToTensor. A detailed description of the data processing and calculation of eigenvalues of thermal expansion tensor is given in detail in (Bubnova *et al*., 2018).

3. Results

3.1. Single-crystal X-ray diffraction

According to the Inorganic Crystal Structure Database (ICSD), there are several works known devoted to a refinement of crystal structure of iron-rich hulsite (Yamnova *et al*., 1975, 1978; Konnert *et al*., 1976). Atomic displacement parameters were refined in isotropic approximation in these works. In this work, atomic displacement parameters for all atoms in the crystal structure of the iron-rich hulsite are refined in anisotropic approximation for the first time. A local environment and oxidation states of Fe and Sn atoms as well as a charge distribution are in accordance with Mössbauer spectroscopy data.

There are five non-equivalent crystallographic octahedral sites for cations in crystal structure of hulsite: the $M(1)$ (1a) site is occupied by Fe^{3+}, $M(2)$ (1f) – by Fe^{2+}, Mg^{2+} and Sn^{4+}, $M(3)$ and $M(4)$ (1d and 1g) by $Fe^{2.5+}$, $M(5)$ (2n) – by Fe^{2+}. The average $M(1)$–O bond length is equal to 2.04 Å, <$M(2)$–O> = 2.16 Å, <$M(3)$–O> and <$M(4)$–O> are equal to 2.08 Å, <$M(5)$–O> = 2.12 Å (Table S3). The <B(1)–O> bond length equals 1.38 Å. Two types of the magnetic subsystems formed by the corner-sharing $M(1)^{3+}$–$M(2)^{2+}$ and $M(3)^{2.5+}$–$M(4)^{2.5+}$ infinite parallel sheets elongated through the b and c directions could be found [Fig 1(a)]. All crystallographic sites are magnetically ordered below 125 K. In the range 125–383 K the $M(3)^{3+}$–$M(4)^{2+}$ subsystem is ordered while the $M(1)^{3+}$, $M(2)^{2+}$ and $M(5)$ sites are in the paramagnetic state. At temperature higher than 383 K all the sites are in the paramagnetic state (see p. 3.2.2 and 3.3).

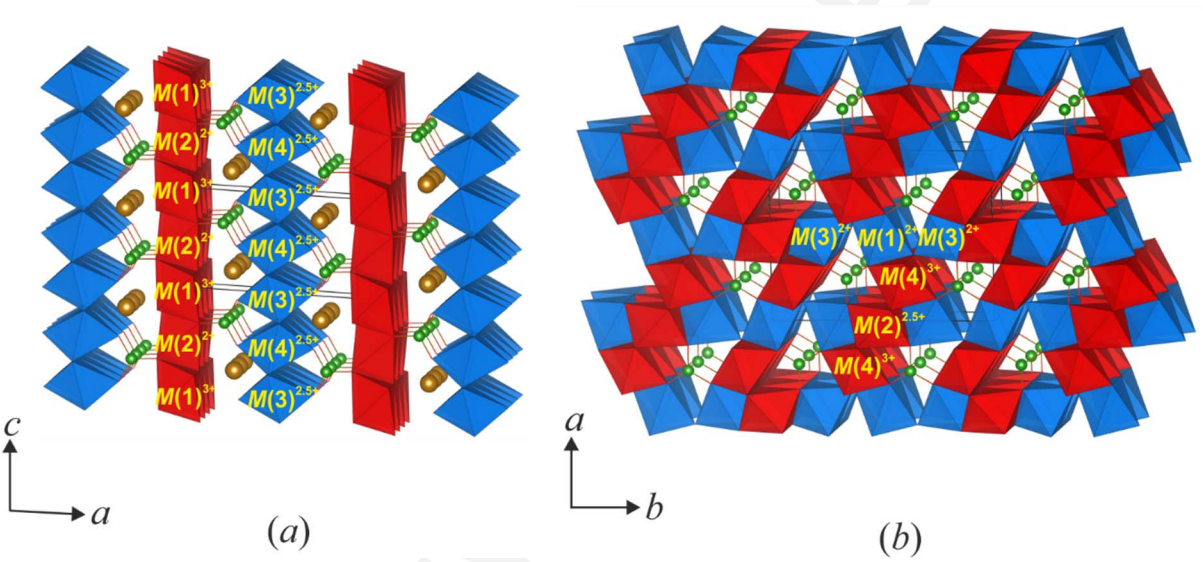

Figure 1 Crystal structures of (a) hulsite and (b) vonsenite with highlighted magnetic subsystems.

Crystal structure of vonsenite was described in details in (Biryukov *et al.*, 2020; CCDC 2004063). Here, a short description is given. It contains four non-equivalent crystallographic sites occupied by the Fe(II,III), Mg^{2+} and Sn^{4+} cations. The $M(1)$ (2a) and $M(3)$ (4g) octahedral sites are occupied by Fe^{2+}, Mg^{2+} and Sn^{4+}, the $M(2)$ (2d) – by $Fe^{2.5+}$, the $M(4)$ (4h) – by Fe^{3+}. The average $M(1)$–O and $M(3)$–O bond lengths are equal to 2.13 Å, <$M(2)$–O> = 2.09 Å, <$M(4)$–O> = 2.06 Å. There are two magnetic subsystems formed by the corner-sharing $M(3)^{2+}$–$M(1)^{2+}$–$M(3)^{2+}$ and edge-sharing $M(4)^{3+}$–$M(2)^{2.5+}$–$M(4)^{3+}$ triads [Fig 1(b)] that is in agreement with reported data for synthetic vonsenite (Guimarães *et al.*, 1999; Bordet & Suard, 2009). A partial magnetic ordering is observed in the temperature range 70–114 K (see p. 3.2.1 and 3.3).

3.2. Mössbauer spectroscopy

3.2.1. The ^{57}Fe and ^{119}Sn Mössbauer spectroscopy of vonsenite

The ^{57}Fe Mössbauer spectra of vonsenite are shown in Fig. 2. It is known that a charge ordering occurs in synthetic vonsenite $Fe^{2+}{}_2Fe^{3+}(BO_3)O_2$ at about 300 K (Guimarães *et al*., 1999; Douvalis *et al*., 2002; Bordet & Suard, 2009). According to previous works Mössbauer spectra below this temperature may be fitted with five components. These components are related with iron atoms occupied four crystallographic sites (2*a*, 2*d,* 4*h*, 4*g*) and one site (4*h*) corresponds to iron ions in the valence states of 2.5+ and 3+ (Bordet & Suard, 2009). With a decrease in temperature, a first magnetic transition occurs at ~114 K. Below this temperature, the components are magnetically splitted, however some part of ferrous ions in the 4*g* sites remains in paramagnetic state. With further decrease in temperature below 70 K (according to magnetometry results, *vide infra*), all sites in the crystal structure of vonsenite are magnetically ordered. Thus, spectrum collected at 25 K consists of only magnetically ordered components. Additionally, minor traces of magnetite (Fe_3O_4) manifest in spectra at the lower temperatures.

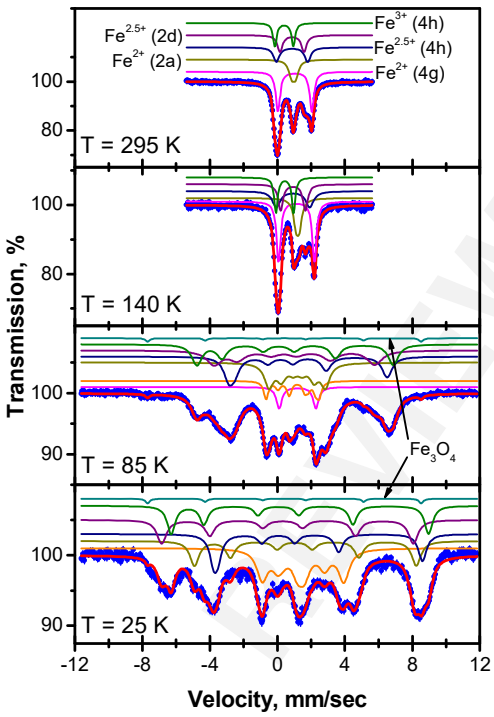

Figure 2 The ^{57}Fe Mössbauer spectra of vonsenite at selected temperatures. Blue dots correspond to experimental data, colored solid lines are model components and red solid curves are their sum.

The ^{119}Sn Mössbauer spectra of vonsenite collected at 295 and 80 K are depicted in Fig. 3. Spectrum at 295 K represents quadrupole doublet with isomer shift of 0.10(3) mm/s and quadrupole splitting of

the order of 0.93(3) mm/s. These values are characteristic for Sn^{4+} in a distorted oxygen environment. We suppose that the Sn impurity ions occupy the 4*g* crystal sites mainly. Magnetically splitted component manifests in the spectrum collected at 80 K. Value of hyperfine field is 51(1) kOe. Since tin is non-magnetic, this field has probably dipole origin, and the Sn^{4+} ions "feel" the magnetic polarization of the neighboring iron ions.

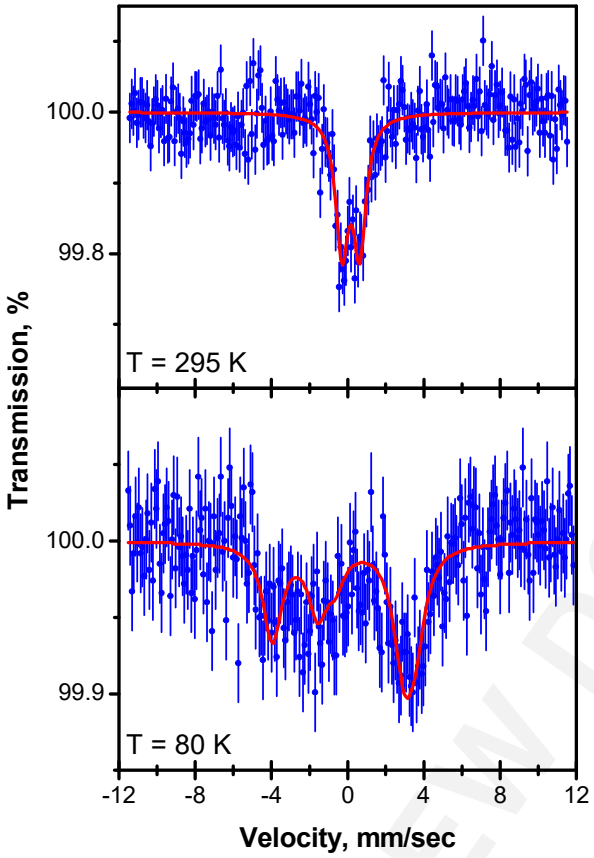

Figure 3 The ^{119}Sn Mössbauer spectra of vonsenite recorded at 295 (top) and 80 K (bottom). Blue dots correspond to experimental data, red solid curves are model fit results.

3.2.2. The ^{57}Fe and ^{119}Sn Mössbauer spectroscopy of hulsite

The ^{57}Fe Mössbauer spectra of hulsite at selected temperatures are shown in Fig. 4. The spectra consist of five major components related with non-equivalent crystallographic sites in the structure of hulsite. It should be noted that additional paramagnetic doublets are required for satisfactory fitting of low temperature spectra. These doublets may be related with paramagnetic impurities and defect centers in the structure. Since the area of these doublets is only a few percent, we will not discuss them further. We will focus on the analysis of the major components only. Additionally, some deviation of line intensities from expected for powder samples is related with texture of samples.

Temperature dependence of isomer shift of iron nuclei in various crystallographic sites are shown in [Fig. 6(*a*)]. Based on estimated isomer shifts values at 5 K we suppose that the 1*a* sites are occupied by the Fe^{3+} ions; the 1*f* and 2*n* sites – by the Fe^{2+}; whereas the 1*d* and 1*g* sites are occupied by the $Fe^{2.5+}$ ions, i.e. the iron ions are in the mixed-valent state. This charge distribution is consistent with charge balance. However, at the temperatures about 200 K some features of isomer shift of the 1*a* and 1*f* components are observed. The value of the isomer shift noticeably increases for the 1*a* site and decreases for the 1*f* site with an increase in temperature. We assume that the observed features are due to delocalization of the 3d electrons on the 1*f* site. As a result of the correlation of the electron density in the crystallographic 1*a* and 1*f* sites, charge density on the 1*f* site increases, because the d-electrons have zero density on nuclei, but they have an influence on charge density on nuclei through shielding of the 3s-electrons. At the same time, charge density on the 1*a* sites decreases. At the higher temperatures, isomer shifts monotonically decrease according to second order Doppler effect.

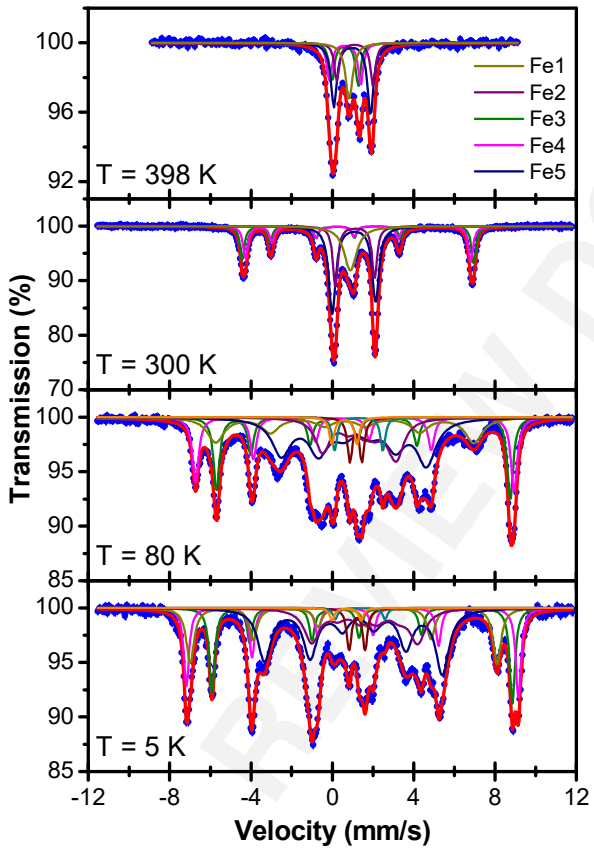

Figure 4 The ^{57}Fe Mössbauer spectra of hulsite at selected temperatures. Blue dots are experimental data, colored solid lines are model components, and red solid curves are their sum.

Temperature dependencies of hyperfine fields on iron nuclei in aforenamed crystallographic sites are shown in [Fig 5(*b*)]. There are at least four peculiarities in this plot. First magnetic transition occurs at 383 K (Biryukov *et al*., 2020). At this temperature iron ions on the 1*d* and 1*g* sites are magnetically ordered. According to magnetometry results (*vide infra*), this ordering has antiferromagnetic origin. However, magnetic moments of these ions are non-compensated, which is observed as small difference of hyperfine fields. With temperature decreasing, the difference also decreases, vanishes at about 200 K and changes the sign with further cooling. The second magnetic transition occurs at ~125 K. At this temperature iron ions on the 1*a*, 1*f*, and 2*n* sites are magnetically ordered. Moreover, hyperfine field on iron nuclei in the 1*g* sites rises, while values for the 1*d* one does not change significantly. The fourth feature corresponds to intersection of hyperfine field dependencies of the 1*a* and 1*d* sites at ~40 K. All these peculiarities manifest itself on magnetization data as will be shown later.

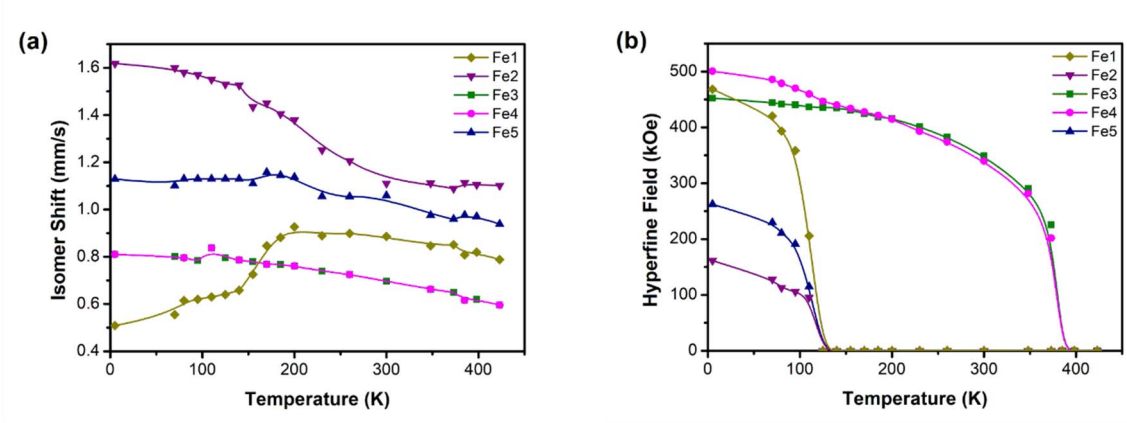

Figure 5 Temperature dependence of hyperfine parameters of ^{57}Fe Mössbauer spectra components of hulsite: (*a*) isomer shift and (*b*) hyperfine field on iron nuclei. Dots correspond to estimated values, and lines are polynomial interpolations for visualization.

The ^{119}Sn Mössbauer spectra of hulsite recorded at several temperatures are shown in Fig. 6. Room temperature spectrum may be fitted by doublet with isomer shift of 0.06(2) mm/s and quadrupole splitting of 0.96(2) mm/s. Hyperfine parameters of the doublet are characteristic for the Sn^{4+} ions. Due to relatively strong quadrupole splitting and value of ionic radius of the Sn^{4+}, which is bigger than the Fe^{3+} radius and lower than the Fe^{2+} radius, these ions may occupy the 1*f* and / or 2*n* sites. With a decrease in temperature, the isomer shift rises according to second order Doppler effect.

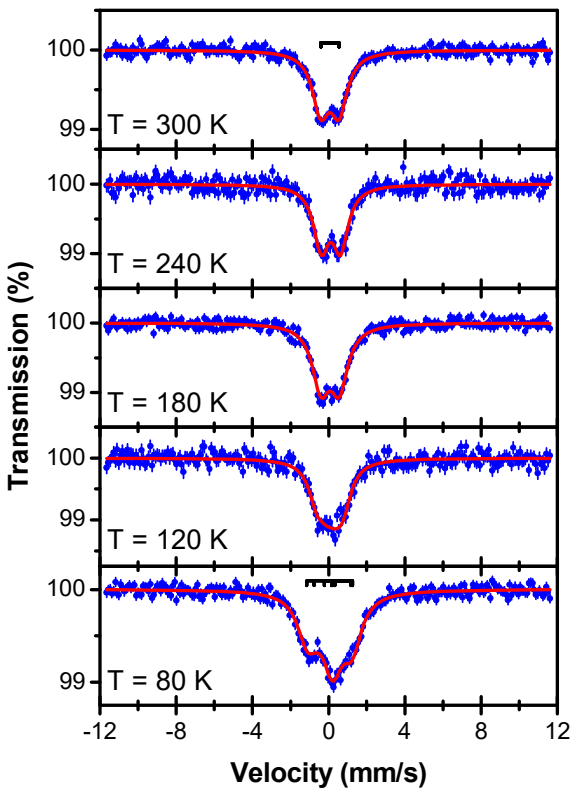

Figure 6 The ^{119}Sn Mössbauer spectra of hulsite at selected temperatures. Blue dots correspond to experimental data, red solid curves are least-squares model fit curve.

Spectra collected at 80 and 120 K show magnetically ordered pattern, and hyperfine magnetic field on the ^{119}Sn nuclei at 80 K is 11.2(3) kOe. Probably the observed magnetic splitting has dipolar origin, and source of this field is magnetically ordered iron ions in the vicinity of tin ions. So far as tin ions start to "feel" the magnetic ordering of iron ions at ~120 K, i.e. at the second magnetic phase transition where the 1*a*, 1*f*, and 2*n* sites are magnetically ordered, it is more likely that the Sn^{4+} atoms are on the 1*f* sites. Temperature dependence of isomer shift shows a minor drop at ~200 K (Fig. 7). It may be another sign of the electron delocalization in the 1*a*-1*f* quasi-plane at this temperature region.

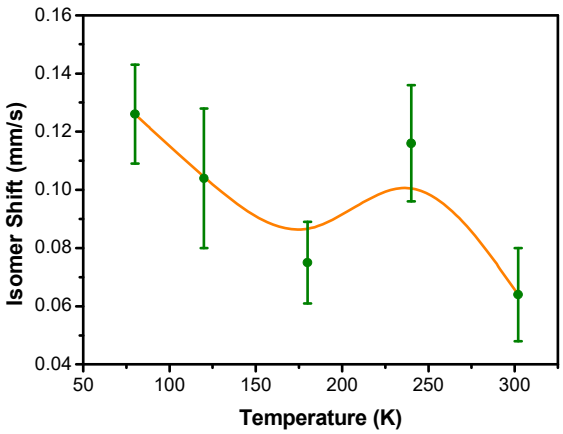

Figure 7 Temperature dependence of the ^{119}Sn Mössbauer isomer shift of hulsite. Green dots are estimated values, orange line is polynomial interpolation for visualization.

3.3. Magnetic properties

Magnetization curves of vonsenite measured in the field-cooled (FC) and zero-field-cooled (ZFC) modes are shown in Fig. 8. First, one should note that a high value of magnetic moment at elevated temperatures is related to the presence of a ferrimagnetic magnetite Fe_3O_4. Moreover, a splitting of the ZFC and FC curves at about 125 K most probably originate from the Verwey transition of this impurity (Walz, 2002). No other magnetic phase transition is known for the magnetite at lower temperatures. Thus, the features observed in the temperature dependence of the sample magnetization below 125 K can be associated with the intrinsic properties of the vonsenite, and the pattern of phase transitions resembles the one reported for the synthetic vonsenite before. It is known that the synthethic vonsenite $Fe^{2+}{}_2Fe^{3+}(BO_3)O_2$ shows several magnetic phase transitions at 114, 70 and 40 K (Douvalis *et al*., 2002; Bordet & Suard, 2009; Martin *et al*., 2017; Damay *et al*., 2020). In this sequence, the magnetic state of the compound changes in the way of paramagnetic-antiferromagnetic-weak ferromagnetic-antiferromagnetic, and between 70 and 114 K paramagnetic and magnetically ordered iron ions coexist. However, an origin of the transition at 40 K is not clear (Bordet & Suard, 2009). Increase of the magnetization at low temperatures reveals a presence of the paramagnetic centers and / or impurities.

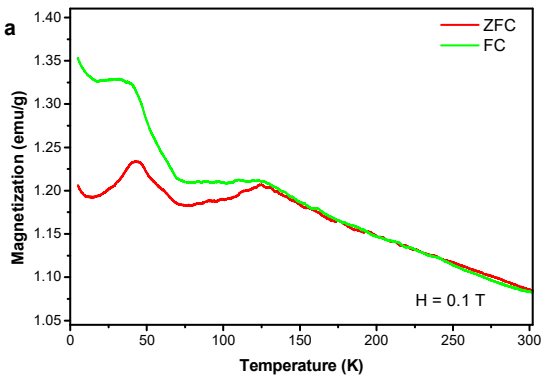

Figure 8 The ZFC-FC magnetization curves of vonsenite.

The magnetization data of hulsite are shown in Fig. 9. To our knowledge, these are the first results on magnetic measurements of iron-rich hulsite. So far, no data on the magnetometry of iron-rich hulsite have been available. However, these results should be treated with some caution since investigated material is natural and its chemical composition contains insignificant amount of the impurities that however should not alter the magnetic properties of hulsite qualitatively as the concentration of the only one magnetic impurity Mn^{2+} is quite low.

From the magnetometry results [Fig. 9(*a*-*b*)], five magnetic transformations of hulsite can be deduced that take place at the temperatures of about 383, 235, 125, 67 and 45 K. Magnetization process at T = 399 K is linear up to 9 T, which is typical for paramagnetic materials. The absence of hysteretic behavior in the field dependence of magnetization at 300 K (see inset in Fig. 9) and low amplitude of the features in M(T) curves both in weak and strong magnetic fields [Fig. 9(*a*,*b*)] indicate an onset of antiferromagnetic-like ordering at 383 K. Moreover, Mössbauer data [Fig. 5(*b*)] show unambiguously that the ordering occurs within the Fe3-Fe4 planes. With further temperature decrease, at about 235 K, the ZFC and FC curves split slightly (see inset in [Fig. 9(*a*)]) reflecting a development of magnetic irreversibility. The second clearly revealed magnetic phase transition occurs at ~125 K, which also coincides with an onset of transformation in Mössbauer spectrum and cell parameters (see p. 3.4). So, in contrast to vonsenite, this magnetic transition is an intrinsic property of hulsite, but not magnetite. Additionally, a small hysteresis of magnetization curve is found at 80 K. Below 125 K hulsite attains an extra non-compensated magnetic moment and shows thus a weak ferromagnetic response. At the temperatures below the third magnetic transition, found at ~ 67 K, magnetization of hulsite rises sharply, reaches its maximum and then falls down with the further temperature decrease. Magnetization field dependence at 60 K shows a clear hysteretic behavior, with the value of remnant magnetization noticeably higher than that at 80 K. The coercivity is about 67 mT. An appearance of such a hysteresis loop reflects a ferrimagnetic-like state of hulsite below 67 K. With decreasing the temperature to 50 K the coercivity reaches a value of 269 mT.

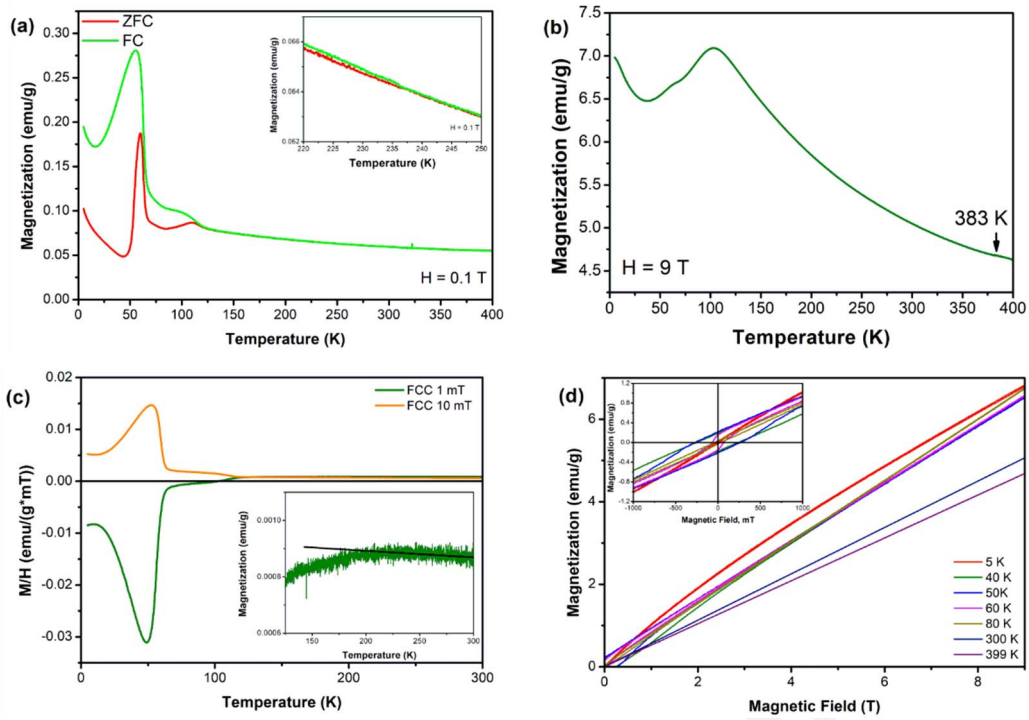

Figure 9 Magnetization data of hulsite: ZFC-FC magnetization curves (*a*), temperature dependence of magnetization of hulsite at high external magnetic field of 9 T (*b*), FCC curve at low external magnetic field (*c*), and field dependence of magnetization of hulsite recorded at selected temperatures (*d*). Insets in (*a*) and (*b*) show corresponding data in finite temperature regions, and inset in (*d*) is the data in the region of low magnetic field.

In our opinion, this may be due to a strong increase of magnetic anisotropy of the system. We suppose that at ~ 45 K the fourth magnetic transition occurs, as a maximal departure between ZFC and FC curves is found at this temperature. Magnetic hysteresis is also observed at 40 K. Remnant magnetization and the saturated moment corresponding to the hysteretic component of magnetic response are close to the ones at 50 K, while the coercive field decreases to 250 mT. Furthermore, the shape of the hysteresis curve changes: its area increased after the sample cooling. Interestingly, with further temperature decrease, the coercivity and remnant moment drop and system restores its weak-ferromagnet/antiferromagnetic-like state. It shows that the magnetic anisotropy is modified as a result of another transformation, either magnetic or structural. It should be noted however that ZFC-FC curves do not converge at low temperatures indicating that hulsite holds its magnetic irreversibility, leaving its overall magnetization history dependent in the whole range of temperatures below 235 K. At low temperatures, the magnetization rises gradually, most probably, due to paramagnetic centers and/or impurities inevitably present in natural hulsite. These paramagnetic centers manifest themselves also in a curved shape of M(H) curve at 5 K.

Another interesting magnetic phenomenon in hulsite is the *negative magnetization* observed in definite experimental conditions. We studied the temperature dependence of magnetization under small positive magnetic field of 1 mT applied upon cooling from 400 K, i.e. starting from fully paramagnetic state. This field-cooled cooling (FCC) curve is shown in [Fig. 9(*c*)] by green. At 125 K, the magnetization starts to decrease, crosses zero at 102 K (magnetic compensation point), prolongs to decreases gradually and at 67 K falls sharply. On further cooling, magnetic moment reaches its minimum at 50 K, and finally increases remaining negative down to 5 K. If the same procedure is performed under an applied field of 10 mT (orange curve in [Fig. 9(*c*)]), no magnetization reversal takes place; the magnetic evolution of the system is almost symmetric with respect to its state at ~ 150 K. Undoubtedly, the observed phenomenon originates from the influence of the already ordered iron-ion subsystem on the one experiencing ordering at 125 K.

Going deeper into details, a key for explanation of the negative magnetization is the uncompensated character of the antiferromagnetic structure established within the Fe3–Fe4 planes below 383 K. Inequality of magnetic moments at the Fe3 and Fe4 sites is clear from the difference of the Mössbauer hyperfine fields [Fig. 5(*b*)]. These ions get magnetically-ordered upon cooling with the larger magnetic moment along the applied magnetic field. However, the balance between the Fe3 and Fe4 moments gradually changes with temperature, and the moment of the Fe4 becomes larger than the Fe3 at ~220–230 K. In the same temperature range the magnetization starts to decrease with temperature (inset to [Fig. 9(*c*)]). In the weak applied magnetic field of 1 mT, this can result in the alignment of the Fe3–Fe4 subsystem net moment antiparallel with respect to the field as the last is not strong enough for magnetization reversal. These magnetic moments create an effective local magnetic field (probably of the exchange anisotropy origin) for the Fe1, Fe2 and Fe5 iron ions that order magnetically at lower temperatures (see [Fig. 5(*b*)]. Consequently, this second magnetic subsystem orders with its non-compensated magnetic moment also antiparallel to the field. This fact is clearly seen on FCC curve. The stronger applied magnetic field obviously overcomes the effective field from the Fe3–Fe4 subsystem, therefore the second (Fe1, Fe2, Fe5) one orders with its moment parallel to the field. Significant changes in M(T) curves observed at 67 K and below, in our opinion, reflect the magnetic evolution of the hulsite as a whole which evidently is rather complicated, demands further investigations and is beyond the scope of the current paper.

3.4. Low temperature X-ray powder diffraction (LTXRD)

LTXRD of vonsenite. Temperature dependencies of unit cell parameters of vonsenite are shown in [Fig. 10(*a*)]. There is a strong negative volume thermal expansion within the range of 93–130 K that is due to a behavior of the *a* and *b* cell parameters. The minimum values of the *a* and *b* parameters are at about 120 K. This temperature is very close to the critical one determined by Mössbauer spectroscopy

and magnetometry (125 K), where the magnetic transition was revealed (see p. 3.2.1 and 3.3). It seems that the volume magnetic ordering takes place up to 125 K could be a reason of such a compression of the structure through the *a* and *b* directions due to a change of the *M*–O bond lengths and / or angles between the [MO_6] polyhedra with a subsequent decrease of the cell parameters. Similar behavior of cell parameters of synthetic compounds near critical temperatures was previously obtained in $Fe_3(BO_4)O_2$, $FeBO_3$ and $SrFe_xTi_{1-x}O_{3-\delta}$ (Biryukov *et al*., 2018; Chezhina *et al*., 2019), $GdFe_3(BO_3)_4$ and $YFe_3(BO_3)_4$ (Frolov *et al*., 2016; Frolov *et al*., 2018), α-$SrCr_2O_4$ (Dutton *et al*., 2011) and $Fe_2(BO_3)O$ (Shimomura *et al*., 2007).

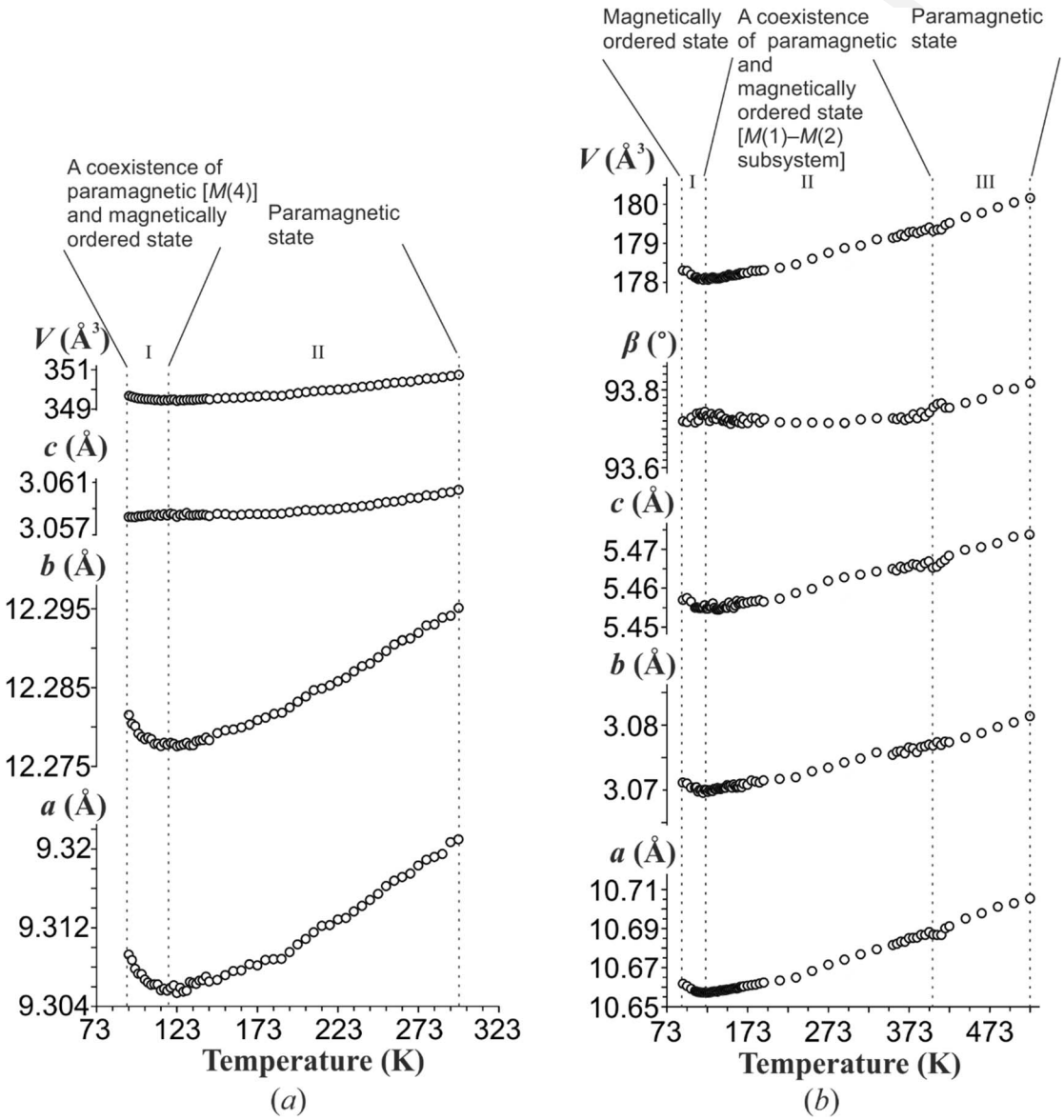

Figure 10 Temperature dependencies of the unit-cell parameters of (*a*) vonsenite and (*b*) hulsite. Intervals of approximation are signed with Romans numerals.

LTXRD of hulsite. As can be seen in [Fig. 10(*b*)], there are two bends on temperature dependencies of unit cell parameters of hulsite. The first distinctive one is within the range 73–150 K with minimal values of the parameters at about 120 K and the second weak one is within the range 390–500 K where a change of the parameters is observed at approximately 390 K. These temperatures differ insignificantly from the critical ones determined by Mössbauer spectroscopy and magnetometry (125 and 383 K, respectively) (see p. 3.2.2 and 3.3).

Our recent works (Biryukov *et al*., 2018; Biryukov *et al*., 2019; Chezhina *et al*., 2019) show that in order to calculate thermal expansion coefficients more accurately the temperature dependencies of unit cell parameters could be divided on several intervals, generally before and after critical temperatures. Thus, the temperature dependencies of the orthorhombic unit cell parameters as well as the volume of vonsenite [Fig. 10(*a*)] were approximated using quadratic polynomials in the temperature ranges 93–115 K (before the magnetic transition) and 115–313 K (after the magnetic transition). An intersection point between these curves is equal to 116.3 K. The calculated thermal expansion coefficients at selected temperatures are given in Table 2. Equations of the approximations are given in Table S4.

Table 2

Thermal expansion coefficients of vonsenite at several temperatures.

α (10^6 °K^{-1})	Temperature (K)						
	93	**105**	**113**	**120**	**130**	**140**	**300**
$\alpha_a = \alpha_{11}$	–34.61(5)	–17.51(1)	–8.91(2)	3.93(3)	4.54(3)	5.14(2)	12.69(2)
$\alpha_b = \alpha_{22}$	–29.11(4)	–14.21(1)	–6.72(2)	3.89(3)	4.37(2)	4.85(2)	10.81(2)
$\alpha_c = \alpha_{33}$	5.31(2)	2.55(6)	1.21(1)	–1.22(2)	–0.71(2)	–0.21(1)	6.18(1)
α_V	–58.3(7)	–29.1(2)	–14.5(4)	6.6(6)	26.8(1)	9.8(4)	29.7(4)

The temperature dependencies of the monoclinic unit cell parameters of hulsite as well as the volume [Fig. 10(*b*)] were approximated using linear approximation in the temperature ranges 93–120 and 120–390 K and quadratic polynomials in the range 390–500 K. The dependencies of the β angle were approximated using linear approximation in the ranges 93–120 K and 390–500 K and quadratic polynomials in the range 120–390 K. Equations of the approximations are given in Table S5. An intersection point between the I and II curves equals 121.5 K, the II and III curves do not intersect. The calculated eigenvalues of thermal expansion tensor of hulsite at selected temperatures are given in Table 3.

Table 3

Eigenvalues of thermal expansion tensor of hulsite at selected temperatures.

α (10^6 °K^{-1})	Temperature (K)						
	93–113	**123**	**200**	**300**	**380**	**400**	**500**
α_{11}	–24.4(3)	8.6(5)	9.1(2)	12.3(2)	15.7(6)	18.5(2)	17.1(2)
$\alpha_b = \alpha_{22}$	–17.1(2)	7.3(4)	7.8(2)	8.6(1)	9.2(3)	8.8(1)	14.2(2)
α_{33}	–9.3(1)	3.9(2)	6.9(2)	8.4(1)	8.6(3)	8.4(1)	6.8(9)
$\mu_{3c} = \angle(\alpha_{33},c)$ (°)	223.7	227.6	207.5	164	157.8	146.6	137.9
α_β	9.2(3)	–2.77(5)	–1.11(2)	1.21(2)	2.92(4)	5.98(6)	5.98(6)
α_a	–16.2(2)	5.8(3)	8.5(1)	12.1(1)	14.9(3)	15.4(2)	13.6(2)
α_c	–16.6(4)	6.4(8)	7.4(3)	8.7(3)	9.7(7)	12.1(3)	11.1(3)
α_V	–50.8(7)	19.9(1)	23.9(5)	29.3(5)	33.6(1)	35.7(5)	38.2(5)

α_{11} and α_{33} – the maximum and minimum thermal expansion coefficients in the monoclinic *ac* plane

4. Discussion

It can be seen in Fig. 11 that there is an expected abrupt change of thermal expansion coefficients of the borates at the critical temperatures that is consistent with thermodynamics on an abrupt change of thermal expansion coefficients as a second-order derivative of Gibbs energy during a magnetic transition (Ehrenfest, 1933). It is seen that the transitions from volume magnetically-ordered state to the paramagnetic one in vonsenite and to the partial magnetically-ordered state in hulsite are accompanied by an abrupt change of eigenvalues of thermal expansion tensor. A change of the eigenvalues of hulsite between the transition from the magnetically-ordered state [the *M*(3)–*M*(4) subsystem] to the paramagnetic one is less sharp.

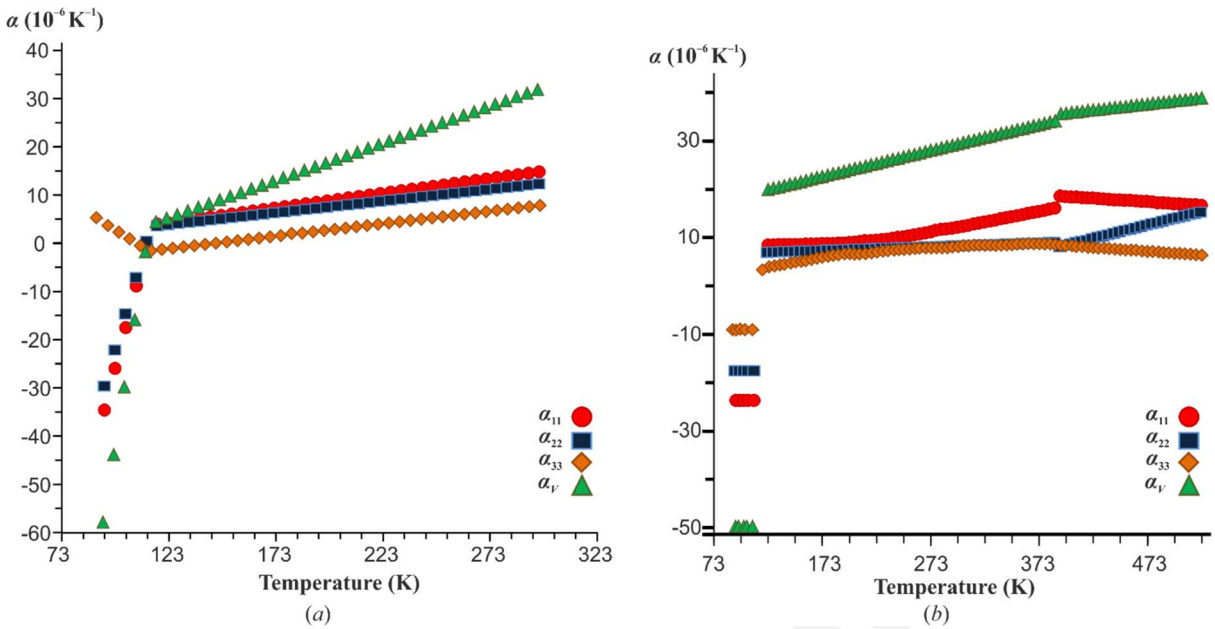

Figure 11 Temperature dependencies of thermal expansion coefficients and eigenvalues of (*a*) vonsenite and (*b*) hulsite.

Thermal expansion of vonsenite. Before the magnetic transition occurred at about 115 K, values of linear (α_{11} and α_{22}) and volume α_V thermal expansion coefficients of vonsenite are negative [Fig. 10(*a*)]. Such a behavior could be caused by magnetostriction or magnetoelastic effects as it was shown for warwickite $Fe_2(BO_3)O$ (Shimomura *et al*., 2007). Only α_{33} values are positive, although they become negative approaching the critical temperature (see [Fig. 10(*a*)] and Table 2). There are the $[BO_3]^{3-}$ triangles located perpendicular to the *c* axis, that should cause a maximum expansion through the *c* axis ($\alpha_{33} = 5.31(2) \times 10^{-6}$ °K^{-1} at 93 K) and minimal in the planes of a preferable orientation of the triangles and strong B–O chemical bonds within them ($\alpha_{11} = -34.61(5)$, $\alpha_{22} = -29.11(4) \times 10^{-6}$ °K^{-1} at 93 K). Such a behavior is consistent with high temperature crystal chemistry of borates (Bubnova & Filatov, 2013). A change of *M*–O bond lengths and / or angles between the $[MO_6]$ polyhedra with a temperature could cause a compression occurred through the *a* and *b* directions. The O(5)–O(4)–O(1) angles [44.54(2)° at 293 K] between the $[M(1)O_6]$ and $[M(3)O_6]$ polyhedra that are equal to as well as the O(3)–O(2)–O(1) [45.91(5)° at 293 K] between the $[M(2)O_6]$ polyhedron and $[M(4)O_6]$ polyhedra (see Fig. 12) could vary with an increase or decrease in temperature during the phase transition. These processes could cause the observed compression through the *a* and *b* directions. After the magnetic transition, values of volume thermal expansion coefficients become positive and the crystal structure expands slightly anisotropically up to room temperature (Fig. 12).

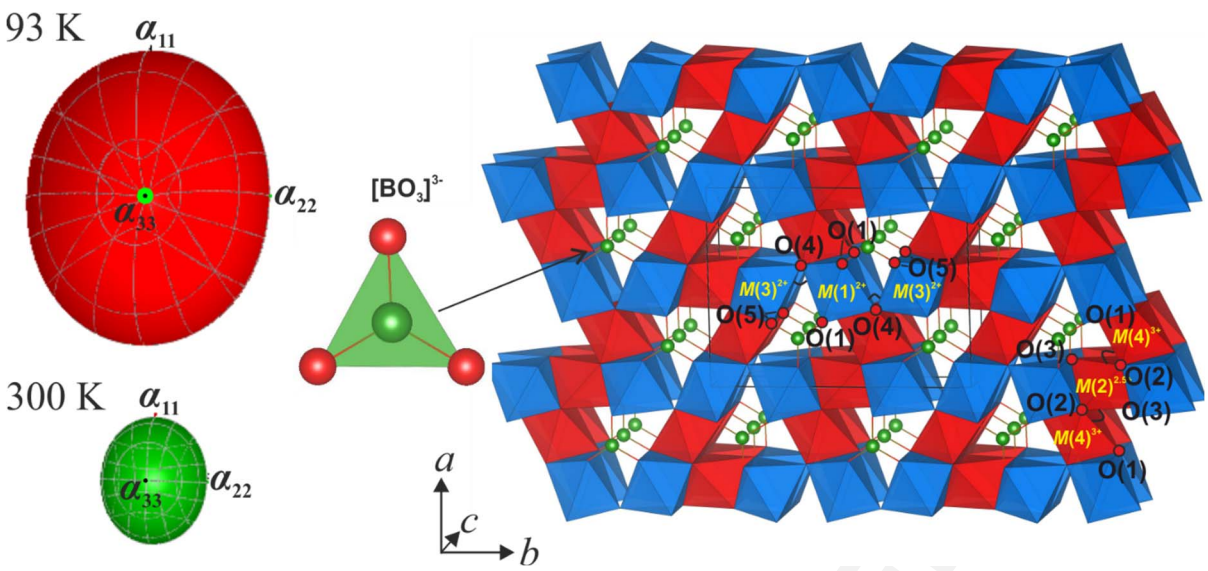

Figure 12 The crystal structure of vonsenite in comparison with figures of thermal expansion at 93 and 300 K (red colored TEC's figure at 93 K shows contraction, green colored at 300K – expansion).

Thermal expansion of hulsite. Thermal expansion of hulsite in the ranges 93–120 and 393–500 K could be described from a viewpoint of shear deformations (Filatov, 2008; Bubnova & Filatov, 2013) – the maximum or minimum thermal expansion should be along one of diagonals of the *ac* parallelogram if the β angle changes. A strong negative volume expansion ($\alpha_V = -79.1(9) \times 10^{-6}$ °K^{-1} at 93 K) is observed up to approximately 120 K where the magnetic phase transition occurs from the volume magnetic ordering to the partial magnetically-ordered state. While the β angle increases the maximum negative thermal expansion is in the direction close to the short diagonal of the *ac* parallelogram in the range 93–120 K ($\alpha_{11} = -33.1(7) \times 10^{-6}$ °K^{-1} at 93 K) (Fig. 13, 93 and 113 K). It is supposed that the volume magnetism takes place in the range 93–120 K which is occurred in all the cationic sites first causes a compression occurred through all the directions of the crystal structure that could be achieved by a change in bond lengths and / or angles. With a further increase in temperature values of linear and volume thermal expansion coefficients become positive (Table 3). In the temperature range 120–390 K the $\Delta\beta$ values do not exceed ~0.02°, thus its thermal expansion could not be described according to the shear deformations theory, although at the first the direction of maximum expansion is close to the short diagonal of the parallelogram and gradually changes with an increase in temperature. The figure of of eigenvalues of thermal expansion tensor smoothly moves clockwise within this region changing a direction of the maximum expansion from the short to the long diagonal of the parallelogram. In the range 390–500 K the direction of the minimum positive thermal expansion is still close to the short diagonal of the parallelogram ($\alpha_{33} = 6.8(9) \times 10^{-6}$ °K^{-1} at 500 K) and maximum expansion is close to the long diagonal of the parallelogram ($\alpha_{11} = 17.1(2) \times 10^{-6}$ °K^{-1} at 500 K).

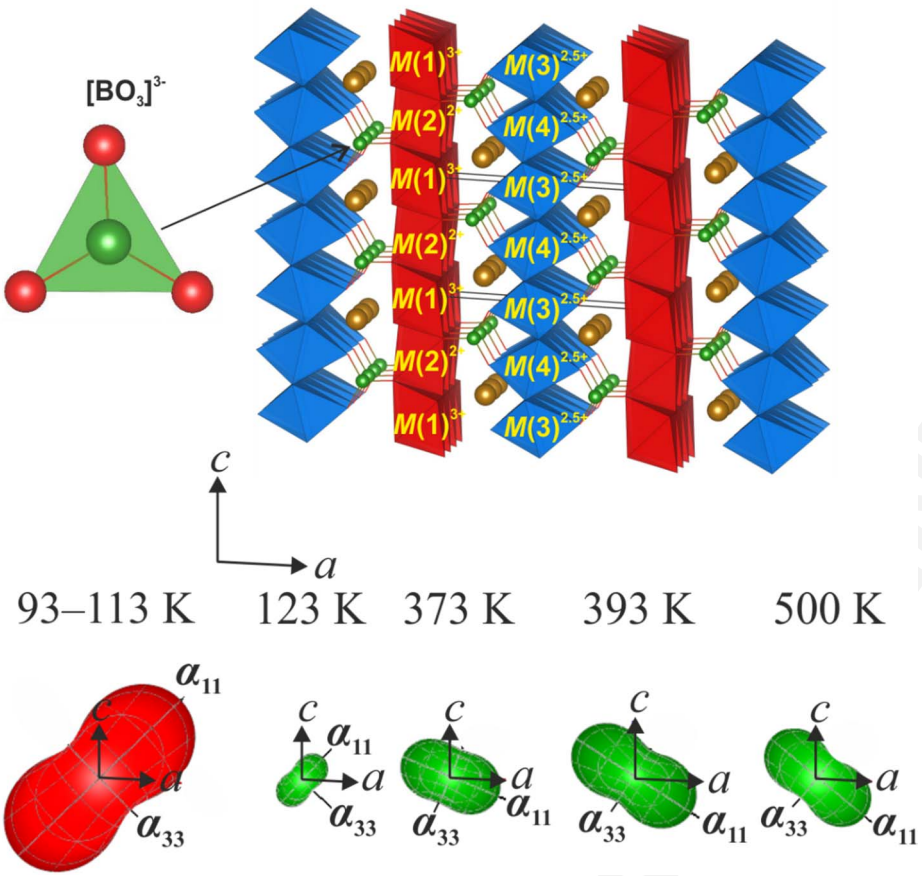

Figure 13 The crystal structure of hulsite in comparison with figures of thermal expansion at several temperatures (red colored TEC's figure at 93–113 K shows negative thermal expansion, green colored at 123–500 K – positive thermal expansion).

5. Conclusion

Iron-rich oxoborates, vonsenite and hulsite crystallize in ludwigite and pinakiolite groups respectively, were investigated by the set of low temperature *in situ* methods including X-ray diffraction, Mössbauer spectroscopy and magnetometry. Crystal structure of hulsite and its atomic displacement parameters were refined from single-crystal X-ray diffraction data in anisotropic approximation for the first time. Cascades of the magnetic transitions with an increase in temperature were found in vonsenite and hulsite in the temperature range 4–500 K. According to the LTXRD data ($93 \leq T \leq 500$ K), all the magnetic phase transitions obtained in this interval are accompanied by an anomalies in cell parameters and thermal expansion coefficients of both oxoborates. An occurrence of the $[BO_3]^{3-}$ triangles plays a significant role in thermal expansion of vonsenite: a maximum expansion is through the *c* axis and a minimal one is perpendicular to the planes of the triangles and strong B–O chemical bonds within them. There is a compression in the *ab* direction of the structure of vonsenite and strong negative volume expansion in the range 93–120 K that could be caused by a change of the

M–O bond lengths and angles between the $[MO]_6$ polyhedra. Shear deformations play a significant role in thermal expansion of monoclinic hulsite in the temperature ranges 93–120 and 393–500 K. The maximum negative thermal expansion is in the direction close to the short diagonal of the *ac* parallelogram in the range 93–120 K. In the range 390–500 K the direction of the minimum positive thermal expansion is still close to the short diagonal of the parallelogram and maximum expansion is close to the longest diagonal of the parallelogram. Due to an insignificant change of the β angle in the temperature range 120–390 K the shear deformations mechanism does not work and the figure of TEC's smoothly moves clockwise changing a direction of the maximum expansion from the short to the long diagonal of the parallelogram.

Acknowledgements The X-ray diffraction experiments were performed at The Centre for X-ray Diffraction Studies (Saint Petersburg State University).

References

Aleksandrov, S.M., Troneva, M.A. (2008). *Geochem. Int.* **46**, 800.

Attfield, J. P., Clarke, J.F. & Perkins, D.A. (1992). *Physica B: Condensed Matter* **180**, 581–584.

Biryukov, Y. P., Filatov, S. K., Vagizov, F. G., Zinnatullin, A. L. & Bubnova, R. S. (2018). *J. Struct. Chem*. **59**, 1980–1988.

Biryukov, Y.P., Bubnova, R.S., Dmitrieva, N.V. & Filatov, S.K. (2019). *Glass. Phys. Chem*. **45** (2), 159–161.

Biryukov, Y.P., Zinnatullin, A.L., Bubnova, R.S., Vagizov, F.G., Shablinskii, A.P., Filatov, S.K., Shilovskikh, V.V. & Pekov, I.V. (2020). *Acta Cryst.* **B76**, 543–553.

Bluhm, K., Müller-Buschbaum, Hk., Walz, L. (1990). *Journal of the Less Common Metals*, **158** (2), 339–345.

Bordet, P., Suard, E. (2009). *Physical Review B: Condensed Matter and Materials Physics* **79**, 144408.

Bubnova, R. S. & Filatov, S. K. (2013). *Z. Kristallogr. Cryst. Mater*. **228**, 395–428.

Bubnova, R. S., Firsova, V. A., Volkov, S. N. & Filatov, S. K. (2018). *Glass Phys. Chem*. **44**, 33–40.

Continentino, M.A., Fernandes, J.C., Guimarães, R.B., Boechat, B. & Saguia, A. (2005). *Magnetism in Highly Anisotropic Borates: Experiment and Theory, Frontiers in Magnetic Materials*, 385–413.

Damay, F., Sottmann, J., Lainé, F., Chaix, L., Poienar, M., Beran, P., Elkaim, E., Fauth, F., Nataf, L., Guesdon, A., Maignan, A. & Martin, C. (2020). *Phys. Rev. B* **101**, 094418.

Douvalis, A. P., Moukarika, A., Bakas, T., Kallias, G. & Papaefthymiou, V. (2002). *J. Phys. Condens. Matter*, **14**, 3303–3320.

Filatov, S. K. (2008). *Physica Status Solidi (B) Basic Research*, **245(11)** 2490–2496.

Freitas, D.C., Continentino, M.A., Guimarães, R.B., Fernandes, J.C., Ellena, J. & Ghivelder, L. (2008). *Phys. Rev. B*. **77**, 184422.

Freitas, D. C., Guimarães, R. B., Fernandes, J. C., Continentino,M. A., Pinheiro, C. B., Resende, J. A. L. C., Eslava, G. G. & Ghivelder, L.(2010). *Phys. Rev. B*, **81**, 174403.

Frolov, K.V., Lyubutin, I.S., Smirnova, E.S., Alekseevsa, O.A., Verin, I.A., Artemov, V.V., Kharlamova, S.A., Bezmaternykh, L.N. & Gudim, I.A. (2016). *Journal of Alloys and Compounds*, 671545–551.

Frolov, K.V., Lyubutin, I.S., Alekseevsa, O.A., Smirnova, E.S., Verin, I.A., Temerov, V.L., Bezmaternykh, L.N., Gudim, I.A., Artemov, V.V. & Dmitrieva, T.V. (2018). *Journal of Alloys and Compounds*. **748**, 989–994.

Galdino, C. W., Freitas, D. C., Medrano, C. P. C., Tartaglia, R., Rigitano, D., Oliveira, J. F., Mendonça, A. A., Ghivelder, L., Continentino, M. A., Sanchez, D. R. & Granado, E. (2019). *Phys. Rev. B,* **100,** 165138.

Guimarães, R. B., Mir, M., Fernandes, J. C., Continentino, M. A., Borges, H. A., Cernicchiaro, G., Fontes, M. A., Candela, D. R. S. & Baggio-Saitovitch, E. M. (1999). *Phys. Rev. B,* **60**, 6617.

Knyazev, Yu.V., Kazak, N.V., Nazarenko, I.I., Sofronova, S.N., Rostovtsev, N.D., Bartolome, J., Arauzo, A.S. & Ovchinnikov, G. (2019). *Journal of Magnetism and Magnetic Materials*. **474**, 493–500.

Konnert, J. A., Appleman, D. A. & Clark, J. R. (1976). *Am. Mineral*. **61**, 116–122.

Krause, L., Herbst-Irmer, R., Sheldrick, G. M. & Stalke, D. (2015). *J. Appl. Cryst*. **48**, 3–10.

Larrea, J. J., Sa´nchez, D. R., Litterst, F. J., Baggio-Saitovitch, E. M., Fernandes, J. C., Guimara˜es, R. B. & Continentino, M. A. (2004). *Phys. Rev. B*, **70**, 174452.

Maignan, A., Lainé, F., Guesdon, A., Malo, S., Damay, F. & Martin, C. (2017). *Journal of Solid State Chemistry*, **246**, 209–213.

Martin, C., Maignan, A., Guesdon, A., Lainé, F. & Lebedev, O.I. (2017). *Inorg. Chem*. **56**(5), 2375–2378.

Matsnev, M. E. & Rusakov, V. S. (2012). *AIP Conf. Proc*. pp. 178–185

Medrano, C. P. C., Freitas, D. C., Passamani, E. C., Resende, J. A. L.C., Alzamora, M., Granado, E., Galdino, C. W., Baggio-Saitovitch, E., Continentino, M. A. & Sanchez, D. R. (2018). *Phys. Rev. B*, **98**,

054435.

Medrano, C. P. C., Sadrollahi, E., Da Fonseca, R. G. M., Passamani, E. C., Freitas, D. C., Continentino, M. A., Sanchez, D. R., Litterst, F. J. & Baggio-Saitovitch, E. (2021). *Phys. Rev. B*, **103**, 064430.

Mir, M., Guimarães, R.B., Fernandes, J.C., Continentino, M.A., Doriguetto, A.C., Mascarenhas, Y.P., Ellena, J., Castellano, E.E., Freitas, R.S. & Ghivelder, L. (2001). *Phys. Rev. Lett*. **87**, 147201.

Momma, K. & Izumi, F. (2011). *J. Appl. Cryst*. **44**, 1272–1276.

Petříček, V., Dušek, Mi. & Palatinus, L. (2014). *Zeitschrift für Kristallographie - Crystalline Materials,* **229**(5), 345–352.

Sasaki, A., Himeda, A., Konaka, H. & Muroyama, N. (2010). *Rigaku J*. **26**, 10–14.

Shimomura, S., Nakamura, S., Ikeda, N., Kaneko, E., Kato, K. & Kohn, K. (2007*). Journal of Magnetism and Magnetic Materials,* **310**, 793–795.

Swinnea, J. S. & Steinfink, H. (1983). *Am. Mineral*. **68**, 827–832.

Takéuchi Y. (1956). *Mineral*. *J*. **2**, 19–26.

Walz, F. (2002). *Journal of Physics: Condensed Matter*. **14**(12), R285.

Whangbo, M., Koo, H. J., Dumas, J. & Continentino, M. A. (2002). *Inorg. Chem*. **41**, 2193–2201.

Yamnova, N. A., Simonov, V. A. & Belov, N. V. (1975). *Sov. Phys. – Crystallogr.*, **20(1)**, 156–159.

Yamnova, N. A., Simonov, V. A. & Belov, N. V. (1978). *Dokl. Akad. Nauk SSSR*, **238**, 1094–1097.

Supporting information

Table S1 Fractional atomic coordinates and equivalent isotropic displacement parameters (Å^2) for hulsite.

Atom	x	y	z	U_{iso}*/U_{eq} (Å^2)	Occupancy
Fe1	0	0	0	0.019 (2)	0.97 (2)
Sn1'	0	0	0	0.019 (2)	0.03 (2)
Fe2	0	0.5	0.5	0.030 (4)	0.6 (2)
Mg2'	0	0.5	0.5	0.030 (4)	0.4 (2)
Fe3	0.5	0	0	0.024 (2)	
Fe4	0.5	0	0.5	0.021 (2)	
Fe5	0.2726 (4)	0.5	0.2210 (6)	0.020 (2)	
O1	−0.6908 (16)	−1	−0.499 (2)	0.019 (4)	
O2	0.4659 (14)	0.5	0.242 (3)	0.019 (4)	
O3	−0.6969 (16)	−1	−0.059 (2)	0.019 (4)	
O4	−0.8872 (13)	−1	−0.291 (3)	0.019 (4)	
O5	0.0922 (17)	0.5	0.182 (3)	0.019 (4)	

Table S2 Anisotropic atomic displacement parameters (Å^2) of hulsite.

Atom	U_{11}	U_{22}	U_{33}	U_{12}	U_{13}	U_{23}
Fe1	0.037 (5)	0.015 (3)	0.003 (6)	0	−0.001 (2)	0
Sn1'	0.037 (5)	0.015 (3)	0.003 (6)	0	−0.001 (2)	0
Fe2	0.045 (7)	0.026 (6)	0.019 (5)	0	−0.005 (3)	0
Mg2'	0.045 (7)	0.026 (6)	0.019 (5)	0	−0.005 (3)	0
Fe3	0.042 (4)	0.010 (3)	0.020 (3)	0	0.004 (3)	0
Fe4	0.024 (4)	0.024 (4)	0.015 (3)	0	0.000 (3)	0
Fe5	0.038 (3)	0.016 (2)	0.007 (3)	0	0.0010 (18)	0
O1	0.031 (8)	0.018 (7)	0.006 (8)	0	−0.001 (3)	0
O2	0.031 (8)	0.018 (7)	0.006 (8)	0	−0.001 (3)	0
O3	0.031 (8)	0.018 (7)	0.006 (8)	0	−0.001 (3)	0
O4	0.031 (8)	0.018 (7)	0.006 (8)	0	−0.001 (3)	0
O5	0.031 (8)	0.018 (7)	0.006 (8)	0	−0.001 (3)	0

Table S3 Selected bond lengths (Å) of hulsite.

Bond	Distance (Å)	BVS	Bond	Distance (Å)	BVS
Fe1—O4^{i}	2.04 (2)	0.46	Fe4—O1^{vi}	2.03 (2)	0.46
Fe1—O4^{ii}	2.04 (2)	0.46	Fe4—O1^{xii}	2.03 (2)	0.46
Fe1—O5^{iii}	2.05 (1)	0.46	Fe4—O2^{iii}	2.10 (1)	0.38
Fe1—O5	2.05 (1)	0.46	Fe4—O2	2.10 (1)	0.38
Fe1—O5^{iv}	2.05 (1)	0.46	Fe4—O2^{xiii}	2.10 (1)	0.38
Fe1—O5^{v}	2.05 (1)	0.46	Fe4—O2^{xiv}	2.10 (1)	0.38
<Fe1—O>$_6$	2.04	2.76	<Fe4—O>$_6$	2.07	2.46
Fe2—O4^{vi}	2.22 (1)	0.26	Fe5—O1^{vi}	2.18 (1)	0.30
Fe2—O4^{vii}	2.22 (1)	0.26	Fe5—O1^{vii}	2.18 (1)	0.30
Fe2—O4^{ii}	2.22 (1)	0.26	Fe5—O2	2.05 (2)	0.43
Fe2—O4^{viii}	2.22 (1)	0.26	Fe5—O3^{i}	2.20 (1)	0.28
Fe2—O5	2.04 (2)	0.42	Fe5—O3^{xv}	2.20 (1)	0.28
Fe2—O5^{ix}	2.04 (2)	0.42	Fe5—O5	1.92 (2)	0.60
<Fe2—O>$_6$	2.16	1.88	<Fe5—O>$_6$	2.12	2.20
Fe3—O2^{iii}	2.07 (1)	0.42	B1—O1	1.36 (2)	1.03
Fe3—O2	2.07 (1)	0.42	B1—O3	1.41 (2)	0.90
Fe3—O2^{x}	2.07 (1)	0.42	B1—O4	1.37 (2)	1.00
Fe3—O2^{xi}	2.07 (1)	0.42	<B—O>$_3$	1.38	2.92
Fe3—O3^{i}	2.10 (2)	0.38			
Fe3—O3^{xii}	2.10 (2)	0.38			
<Fe3—O>$_6$	2.08	2.43			

Table S4 Equations of approximation of temperature dependencies of unit cell parameters of vonsenite.

T (K)	Equation $l(t) = l_0 + l_1t + l_2t^2$			
	***a*(*t*) (Å)**	***b*(*t*) (Å)**	***c*(*t*) (Å)**	***V*(*t*) (Å^3)**
93–115	9.3771(1) – 0.001221(2)×t + 0.0000052(1)×t^2	12.3791(2) – 0.00179(3)×t + 0.0000079(2)×t^2	3.0555(3) + 0.000043(6)×t – 0.00000016(3)×t^2	354.66(9) – 0.0921(2)×t + 0.000404(8)×t^2
115–313	9.3051(6) – 0.000027(6)×t + 0.00000027(2)× t^2	12.2758(7) – 0.000016(7)×t + 0.00000028 (2)×t^2	3.0599(1) – 0.000021(1)×t – 0.000000077(3)×t^2	349.53(3) – 0.0039(4)×t + 0.000027(1)×t^2

Table S5 Coefficients of approximation of temperature dependencies of unit cell parameters of hulsite.

T (K)	Equation $l(t) = l_0 + l_1t + l_2t^2$				
	***a*(*t*) (Å)**	***b*(*t*) (Å)**	***c*(*t*) (Å)**	***β*(*t*) (°)**	***V*(*t*) (Å^3)**
93–120	10.6773(2) – 0.000173(3)×t	3.0759(9) – 0.000052(9)×t	5.4655(2) – 0.000091(2)×t	93.635(3) + 0.86(2)×t	179.14(1) – 0.0091(1)×t
120–390	10.6521(6) + 0.000016(6)×t + 0.00000018(3) ×t^2	3.0673(4) + 0.000018(4)×t + 0.000000012(7)×t^2	5.4506(9) + 0.000028(8)×t + 0.000000032(1)×t^2	93.778(9) – 0.51(9)×t + 1.03(2)×t^2	177.71(5) + 0.0024(4)×t + 0.0000047(8)×t^2
390–523	10.5721(5) + 0.000391(2)×t – 0.00000026(2) ×t^2	3.0781(1) – 0.000033(5)×t + 0.000000012(7)×t^2	5.4506(9) + 0.000028(8)×t + 0.000000077(6)×t^2	93.523(2) + 0.56(5)×t	176.41(2) + 0.0077(9)×t – 0.0000011(1)×t^2